Relativistic cross sections of positron-impact ionization of hydrogenic ions

Tien-Yow Kuo,* Chi-ming J. Chen, Shih-Wei Hsu, and Keh-Ning Huang
Institute of Atomic and Molecular Sciences, Academia Sinica, P.O. Box 23-166, Taipei, Taiwan 106, Republic of China and Department of Physics, National Taiwan University, Taipei, Taiwan 106, Republic of China
(Received 1 June 1992; revised manuscript received 1 March 1993)

Relativistic total and single-differential cross sections of positron-impact ionization are calculated for the hydrogen atom and hydrogenlike ions for incident positron energies up to 10 times the ionization energy. Two different sets of distorting potentials are used to study the mutual screening of the outgoing positron and electron. Relativistic effects are investigated by taking the nonrelativistic limit. Results are compared with available theoretical and experimental data.

PACS number(s): 34.80.Dp, 25.30.Hm

I. INTRODUCTION

Impact ionization of atoms or ions by charged particles is important for diagnostics of high-temperature plasmas as well as for fundamental understanding of atomic structure and collision mechanisms. The positron-impact ionization, in particular, is a good testing ground for the "scattering of electrons without exchange," and with the great improvement in the intensity of positron beams, positron-impact ionization processes have acquired more emphasis than before.

Burke and Taylor [1] obtained the total cross sections for positron-impact ionization of the hydrogen atom by using the first-Born approximation. Various models of the interaction potential within the distorted-wave formalism were used by Ghosh, Mazumdar, and Basu [2] and by Mukherjee and co-workers [3,4] to calculate the total cross sections for positron-impact ionization of hydrogen. In addition to the above nonrelativistic quantum-mechanical calculations, the classical-trajectory Monte Carlo method was also applied to the positron-impact ionization of hydrogen by Ohsaki *et al.* [5] and by Wetmore and Olson [6]. Threshold ionization of hydrogen and hydrogenlike ions was studied by Wetmore and Olson [6], by Klar [7] and by Campeanu *et al.* [8]. Experimental cross sections for positron-impact ionization of hydrogen were measured indirectly by Spicher *et al.* [9] Campeanu *et al.* [10] studied the positron-impact ionization of helium by using the distorted-wave method. A brief report of the physics of low-energy positron collisions was given by Charlton [11].

In this paper, we investigate the cross sections for positron-impact ionization of the hydrogen atom and ions in the hydrogen isoelectronic sequence by using the two-potential distorted-wave approximation in a relativistic framework. Preliminary results for the hydrogen atom have been reported [12]. In Sec. II, we establish the relativistic formulation of positron-impact ionization and use two different sets of distorting potentials to calculate the positron-impact ionization cross sections. In Sec. III, our results are discussed and compared with available experimental data and with those from other theories.

II. RELATIVISTIC FORMULATION OF POSITRON-IMPACT IONIZATION

In the positron-impact ionization processes, we denote the linear momentum and energy of the incident positron by k_i and E_i, respectively. Before the collision, the target is in its ground state with only one electron. After the collision, the target is deprived of its electron and becomes a bare nucleus. The outgoing positron and electron are described by $(k_p E_p)$ and $(k_e E_e)$. We note that all quantities in this paper are given in atomic units.

By energy conservation, we have

$$E_i + E_b = E_p + E_e \ , \tag{1}$$

where E_b is the energy of the bound electron. From scattering theory, it follows that

$$\frac{d^3\sigma}{dE_e d\Omega_p d\Omega_e} = \frac{(2\pi)^4}{c^6}\left[\frac{k_p E_p k_e E_e E_i}{k_i}\right]|T_{fi}|^2 \ , \tag{2}$$

where T_{fi} denotes, symbolically, the transition matrix element. By integrating the triply differential cross sections over Ω_p and Ω_e, we obtain the following expression for the single-differential cross section, which is similar to the expression for electron-impact ionization [13],

$$\frac{d\sigma}{dE_e} = \frac{2\pi^3}{k_i^2(2j_b+1)}\overline{\sigma} \ , \tag{3}$$

where

$$\overline{\sigma} = \sum_{k_i,k_e,k_p,J} d_\alpha^2 \ . \tag{4}$$

Here, the summation is over all possible channels, and the real amplitude d_α is defined by the reduced matrix element of the partial-wave amplitude in channel α, i.e.,

$$d_\alpha \exp(i\delta_\alpha) = i^{l_i-(l_p+l_e)}\exp[i(\sigma_{k_p}+\sigma_{k_e})] \times \langle \alpha^-(j_e j_p)J \| H_I \| (j_b j_i)J \rangle \ , \tag{5}$$

where H_I denotes symbolically the appropriate interaction.

The total cross sections can be calculated as

$$\sigma=\int_{c^2}^{E_i+E_b-c^2}\frac{d\sigma}{dE_e}dE_e \ , \tag{6}$$

where c^2 is the rest energy of the electron or positron, and c is the speed of light. The total Hamiltonian H of the projectile-target system is assumed to be

$$H=(c\alpha_1\cdot p_1+c^2\beta_1)+(c\alpha_2\cdot p_2+c^2\beta_2)+\frac{Z}{r_1}-\frac{Z}{r_2}-\frac{1}{r_{12}} \ . \tag{7}$$

where α_i and β_i are Dirac matrices, and the speed of light c equals the inverse of the fine-structure constant in atomic units. Here r_1 and r_2 refer to the spatial coordinates of the positron and electron, respectively. The total Hamiltonian can be separated into two parts for the initial state,

$$H=H_i+V_i \ , \tag{8}$$

where

$$H_i=(c\alpha_1\cdot p_1+c^2\beta_1)+(c\alpha_2\cdot p_2+c^2\beta_2)-\frac{Z}{r_2} \ , \tag{9}$$

$$V_i=\frac{Z}{r_1}-\frac{1}{r_{12}} \ . \tag{10}$$

The transition matrix element for positron-impact ionization is given exactly by

$$T_{fi}=\langle\Psi_f^{(-)}(r_1,r_2)|V_i|\phi_i(r_1,r_2)\rangle \ , \tag{11}$$

where $\phi_i(r_1,r_2)$ is the initial-state wave function for a positron impinging upon the bound electron in hydrogen, and $\Psi_f^{(-)}(r_1,r_2)$ is the final-state wave function with the incoming-wave boundary condition for the outgoing positron and electron. These wave functions satisfy the following equations:

$$(H_i-E_i-E_b)\phi_i(r_1,r_2)=0 \ , \tag{12}$$

$$(H-E_p-E_e)\Psi_f^{(-)}(r_1,r_2)=0 \ . \tag{13}$$

In the two-potential formulation [14,15], we separate the interaction potential V_i into the distorting potential U_i and the residual potential W_i as

$$V_i=U_i+W_i \ . \tag{14}$$

Because in the initial state the incident positron is screened by the bound electron, we may well choose

$$U_i=\frac{Z}{r_1}-V_b(r_1)+V_{\rm pol}(r_1) \ , \tag{15}$$

$$W_i=-\frac{1}{r_{12}}+V_b(r_1)-V_{\rm pol}(r_1) \ . \tag{16}$$

Here the average potential $V_b(r_1)$ due to the bound electron $\phi_b(r_2)$ is evaluated by

$$V_b(r_1)=\left\langle\phi_b(r_2)\left|\frac{1}{r_{12}}\right|\phi_b(r_2)\right\rangle \ . \tag{17}$$

The charge density of the bound electron is also polarized by the incident positron. In order to take account of the polarization effect, the dipole component in the polarization potential of Temkin and Lamkin [16] is incorporated in the distorting potential for the positron,

$$V_{\rm pol}(r_1)=-\frac{9}{4x^4}[1-e^{-2x}(1+2x+2x^2+\tfrac{4}{3}x^3+\tfrac{2}{3}x^4+\tfrac{4}{27}x^5)] \ . \tag{18}$$

with $x=Zr_1$. The distorted-wave function $\chi_i^{(+)}(r_1)$ with the outgoing-wave boundary condition for the incident positron satisfies the Dirac equation with the distorting potential U_i. Consequently, we may reduce the transition matrix element (11) into the two-potential form as

$$T_{fi}=\langle\Psi_f^{(-)}(r_1,r_2)|W_i|\chi_i^{(+)}(r_1)\phi_b(r_2)\rangle \ . \tag{19}$$

We approximate the final-state wave function by distorted-wave functions for the outgoing positron and electron as

$$\Psi_f^{(-)}(r_1,r_2)\approx\chi_p^{(-)}(r_1)\chi_e^{(-)}(r_2) \ , \tag{20}$$

which satisfy Dirac equations with distorting potentials U_p and U_e, respectively. The choices of the distorting potentials are given explicitly for the present two-potential distorted-wave models (TPDW) as follows.

A. TPDW01

The scattered positron is entirely screened in the asymptotic region by the ejected electron which itself is unscreened, i.e.,

$$U_p=\frac{Z}{r_1}-V_b(r_1)+V_{\rm pol}(r_1) \ , \tag{21}$$

$$U_e=-\frac{Z}{r_2} \ , \tag{22}$$

where U_p and U_e represent the distorting potentials for the outgoing positron and electron, respectively. The numbers 0 and 1 in the notation TPDW01 stand for the absolute values of the asymptotic charges experienced by the outgoing positron and electron, respectively, in the case of hydrogen.

B. TPDW11

Both the scattered positron and the ejected electron are unscreened, i.e.,

$$U_p=\frac{Z}{r_1} \ , \tag{23}$$

$$U_e=-\frac{Z}{r_2} \ . \tag{24}$$

Here again, the numbers 1 and 1 in the notation TPDW11 stand for the absolute values of the asymptotic charges experienced by the outgoing positron and electron, respectively, in the case of hydrogen. The distorting potentials and asymptotic charges for the scattered positron and ejected electron in models TPDW01 and TPDW11 are summarized in Table I.

TABLE I. Distorting potentials and asymptotic charges for the scattered positron and ejected electron in models TPDW01 and TPDW11.

	Distorting potential		Asymptotic charges	
Model	U_p	U_e	Z_p	Z_e
TPDW01	$\frac{Z}{r_1}-V_b(r_1)+V_{\rm pol}(r_1)$	$-\frac{Z}{r_2}$	$Z-1$	Z
TPDW11	$\frac{Z}{r_1}$	$-\frac{Z}{r_2}$	Z	Z

III. RESULTS AND DISCUSSION

To compare single-differential and total cross sections of different ions, we use the threshold energy units, $u_i=(E_i-c^2)/I$, $u_p=(E_p-c^2)/I$, and $u_e=(E_e-c^2)/I$, measured with respect to the rest energy of the electron. Here, I denotes the ionization potential of the particular ion in consideration and is given by $c^2[\sqrt{1-(Z\alpha)^2}-1]$. Also, we make use of reduced cross sections defined as

$$\left[\frac{d\sigma}{dE_e}\right]_{\rm reduced}=Z^6\frac{d\sigma}{dE_e}\ ,$$

$$\sigma_{\rm reduced}=Z^4\sigma\ .$$

We have calculated single-differential cross sections for H I at $u_i=1.1$, 3, and 10 and for He II at 1.1, 4, and 10. Total cross sections for H I, He II, C VI, Ne X, Na XI, Ar XVIII, Fe XXVI, and Ag XLVII and their nonrelativistic limits are also evaluated for u_i ranging from 1.001 to 10. In this paper, we present only selected results.

From Figs. 1–3 we present the single-differential cross sections for H I at $u_i=1.1$, 3, and 10, respectively. In Fig. 1 both TPDW01 and TPDW11 curves decrease with u_e slowly. The TPDW01 curve is much higher than the TPDW11 curve because of the screening effect. In Fig. 2 both TPDW01 and TPDW11 curves decrease with u_e more rapidly. Apparently, the ejected electron is likely to have a much lower velocity than the scattered positron at high incident energies because the interaction time for collisions away from the threshold is much shorter than near the threshold. Comparing the TPDW01 curve with the TPDW11 curve, we find that the screening effect enhances the total cross sections because it, in general, leads to a shorter mean distance between the positron and electron, and the energy transfer between them is more likely to occur. However, this enhancement decreases with the incident energy as shown in Figs. 1–3. This can be understood from the following property of the Coulomb wave function. Because the Coulomb wave function depends on Z only through the parameter Z/k, it is insensitive to changes in Z when the momentum k is high. Consequently, the different asymptotic charges for the positron in the TPDW01 and TPDW11 models do not result in significantly different cross sections at high incident energies. By comparing Fig. 2 with Fig. 3, we also find that the decrease of the single-differential cross section with u_e in Fig. 3 is more rapid than in Fig. 2 because of the shorter collision time at higher incident energies. We also note that the total cross section comes mainly from the low-u_e region. In other words, an uneven sharing of the available kinetic energy (u_i-1) is more favorable at high incident energies.

From Figs. 4–6 we present the single-differential cross sections for He II at $u_i=1.1$, 4, and 10, respectively. In Fig. 4 the decrease of the TPDW01 curve is more rapid than that in Fig. 1 because of the shorter collision time for He II. Due to a smaller relative screening effect for

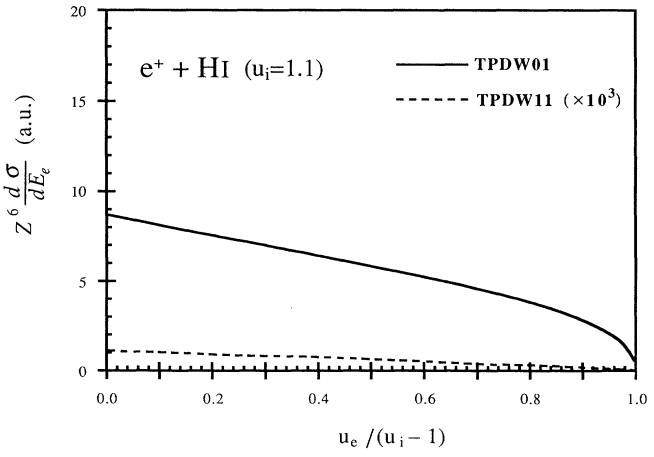

FIG. 1. Reduced single-differential cross sections (in a.u.) for H I at the incident energy $u_i=1.1$ (in threshold energy units).

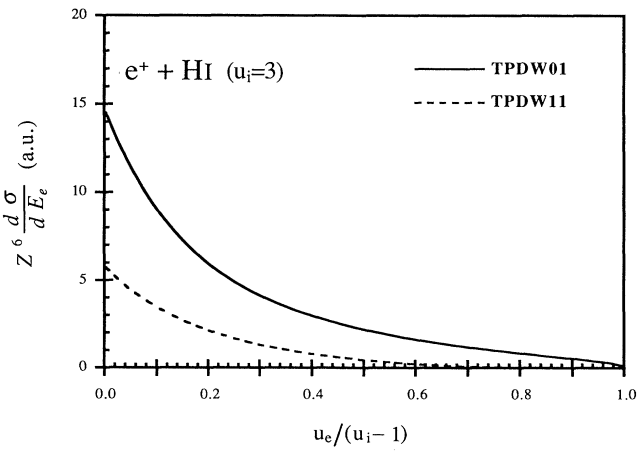

FIG. 2. Reduced single-differential cross sections (in a.u.) for H I at the incident energy $u_i=3$ (in threshold energy units).

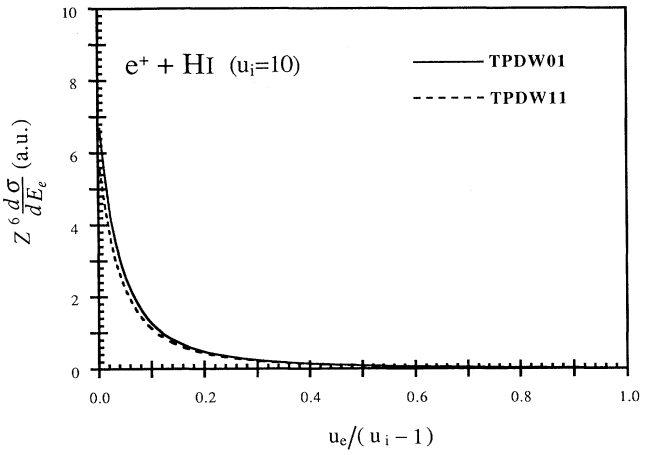

FIG. 3. Reduced single-differential cross sections (in a.u.) for H I at the incident energy $u_i = 10$ (in threshold energy units).

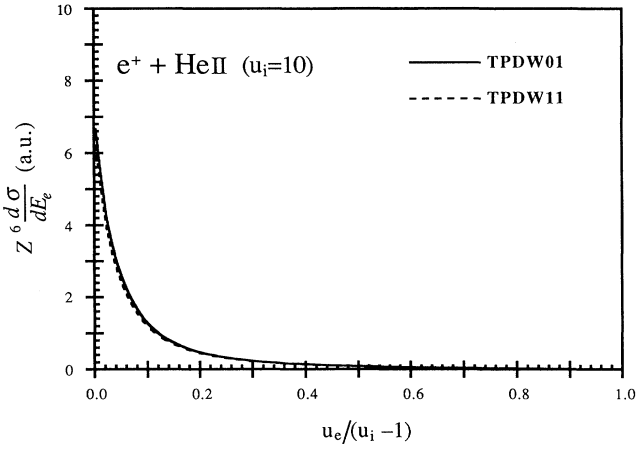

FIG. 6. Reduced single-differential cross sections (in a.u.) for He II at the incident energy $u_i = 10$ (in threshold energy units).

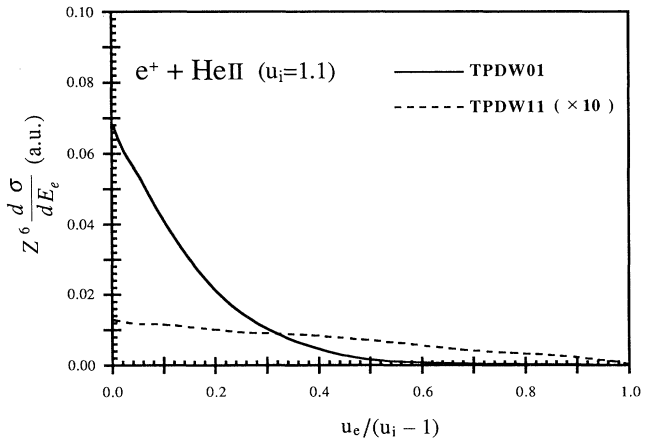

FIG. 4. Reduced single-differential cross sections (in a.u.) for He II at the incident energy $u_i = 1.1$ (in threshold energy units).

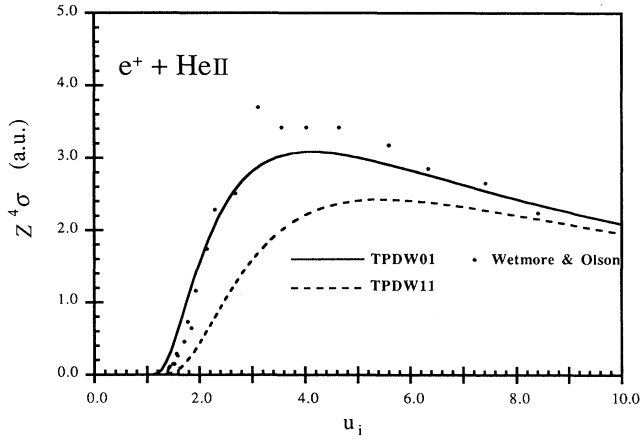

FIG. 7. Reduced total cross sections (in a.u.) for He II. TPDW01 (——) and TPDW11 (— — —): the present results. (●): Classical-trajectory Monte Carlo results of Wetmore and Olson [Ref. 6].

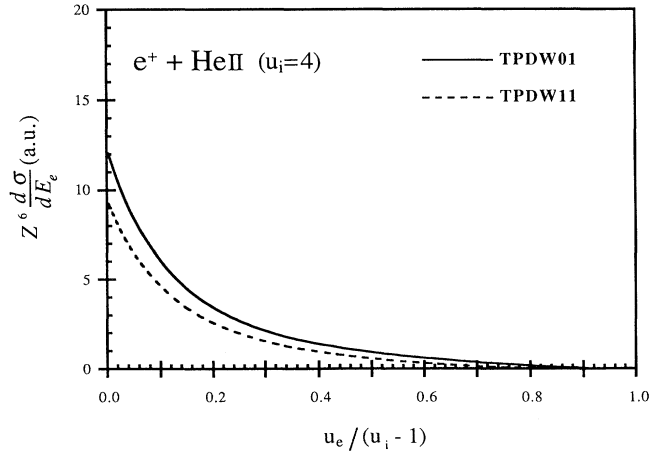

FIG. 5. Reduced single-differential cross sections (in a.u.) for He II at the incident energy $u_i = 4$ (in threshold energy units).

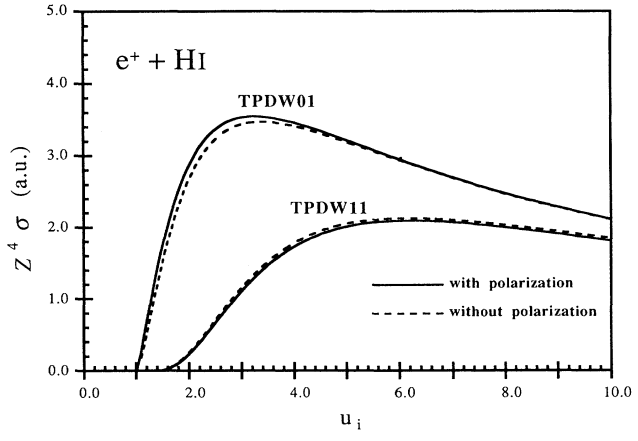

FIG. 8. Reduced total cross sections (in a.u.) with and without the polarization effect for H I.

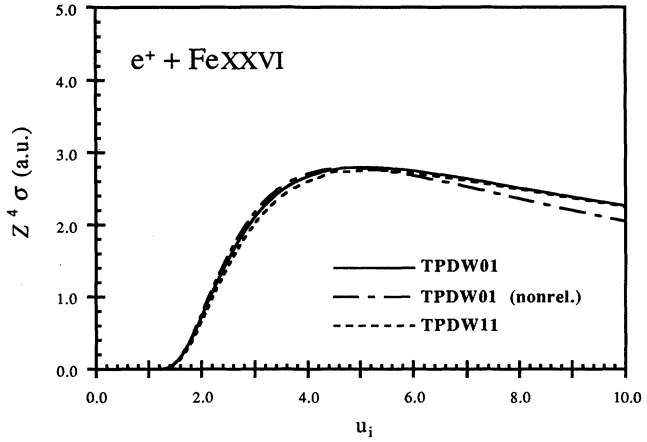

FIG. 9. Reduced total cross sections (in a.u.) for Fe XXVI.

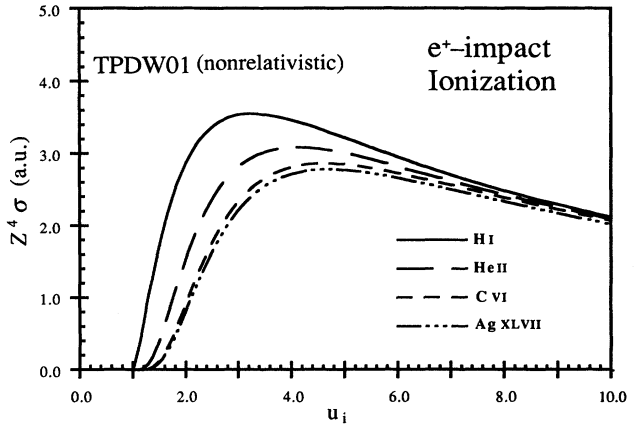

FIG. 12. Nonrelativistic reduced total cross sections (in a.u.) in model TPDW01 for H I, He II, C VI, and Ag XLVII.

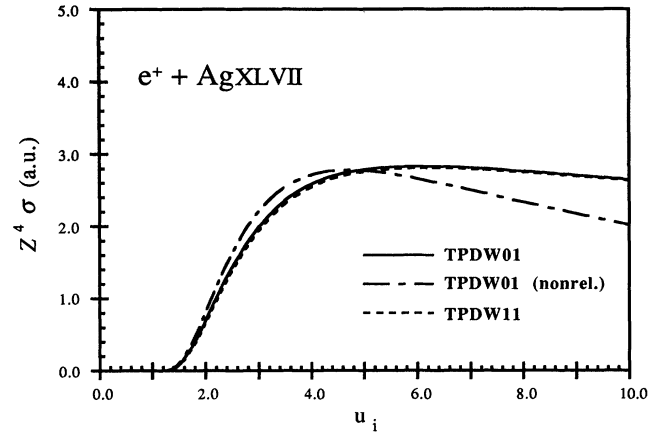

FIG. 10. Reduced total cross sections (in a.u.) for Ag XLVII.

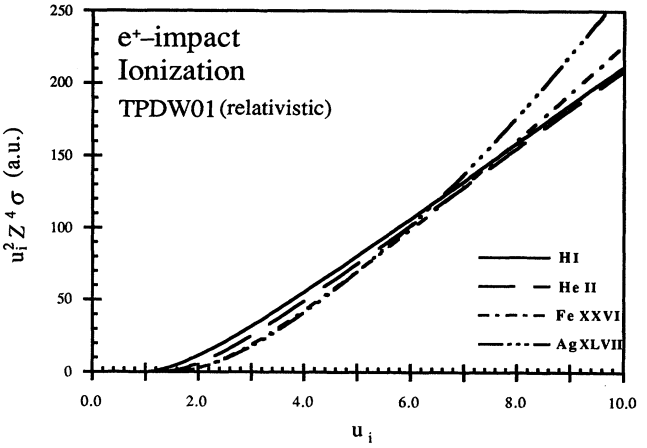

FIG. 13. Reduced total cross sections multiplied by u_i^2 (in a.u.) in model TPDW01 for H I, He II, Fe XXVI, and Ag XLVII.

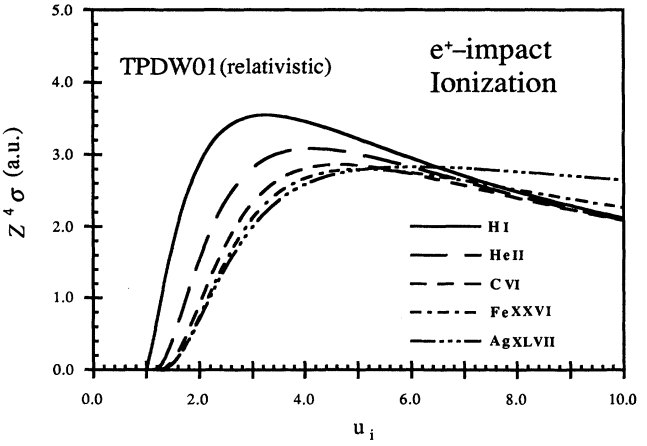

FIG. 11. Reduced total cross sections (in a.u.) in model TPDW01 for H I, He II, C VI, Fe XXVI, and Ag XLVII.

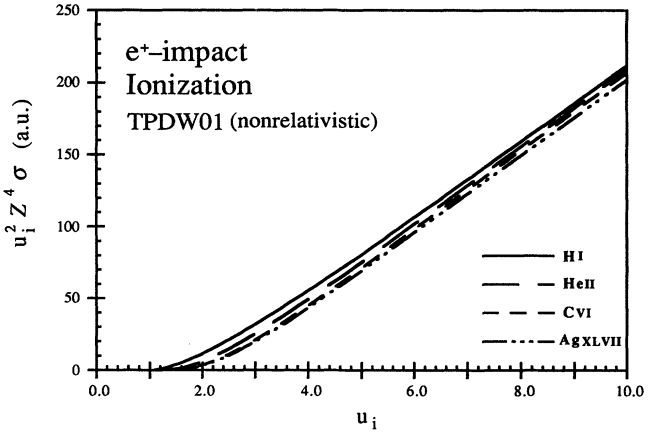

FIG. 14. Nonrelativistic reduced total cross sections multiplied by u_i^2 (in a.u.) in model TPDW01 for H I, He II, C VI, and Ag XLVII.

He II, the difference between the TPDW01 and TPDW11 curves in Fig. 4 is also smaller than that in Fig. 1. In Figs. 5 and 6, the characteristics of the TPDW01 and TPDW11 curves are similar to those in Figs. 2 and 3 except for a smaller difference between the TPDW01 and TPDW11 curves.

The comparison of our total cross sections for H I with the experimental data of Spicher *et al.* [9], the first-Born approximation results of Burke and Taylor [1], the distorted-wave results of Ghosh, Mazumdar, and Basu [2] and of Mukherjee *et al.* [4], and the classical-trajectory Monte Carlo results of Ohsaki *et al.* [5] and of Wetmore and Olson [6] has been presented in a previous paper [12]. There are discrepancies not only between theoretical and experimental data but also among theoretical results. Comparing theoretical results with the experimental data, we find the indirect measurement of the total cross sections of Spicher *et al.* [9] lies far above all theoretical predictions except near the threshold. Direct measurement of the total cross sections of positron-impact ionization of hydrogen is required to resolve this discrepancy.

In Fig. 7 we display the total cross sections for He II, compared with the classical-trajectory Monte Carlo results of Wetmore and Olson [6]. As expected, the TPDW01 and TPDW11 results come closer at higher incident energies. Because of the higher nuclear charge, the deviations among theoretical results for He II are less than those for H I. Further experimental and theoretical studies of He II are also needed.

The polarization of the charge density of the bound electron induced by the incident positron has a small effect on the total cross sections as demonstrated in Fig. 8 for H I. The polarization potential has an even less effect on the total cross sections for He II, and the results with and without polarization are almost discernible. For higher-Z ions, the polarization effect on the total cross section is negligibly small.

The total cross sections for Fe XXVI and Ag XLVII are displayed in Figs. 9 and 10, respectively. The nonrelativistic TPDW01 curves are also presented in these figures. The relativistic effect in the total cross sections becomes discernible for ions beyond Na XI in the hydrogen isoelectronic sequence. With the increase of the nuclear charge, the relativistic effect becomes more significant and the screening effect less important. In Fig. 10 the deviation of the relativistic TPDW01 curve from the nonrelativistic one is more prominent because of the larger relativistic effect in Ag XLVII. The relativistic effect tends to reduce the total cross sections for the low incident energies and enhance the total cross sections for high incident energies. The screening effect becomes negligible in Ag XLVII because of the higher nuclear charge Z.

To study the systematics of total cross sections of positron-impact ionization along the hydrogen isoelectronic sequence, we plot the TPDW01 results for all ions in Fig. 11. The total cross sections for H I and He II deviate from the general trend at low incident energies because of the screening effect and for Fe XXVI and Ag XLVII at high incident energies because of the relativistic effect. This general trend is more apparent for nonrelativistic TPDW01 cross sections which are presented in Fig. 12. For ions after C VI, the nonrelativistic TPDW01 curves are almost indistinguishable from each other such that they form a universal curve. This general trend is also followed nicely for the TPDW11 results, which do not include the screening effect. In Figs. 11 and 12, Thomson's scaling law [17] manifests itself in the quantum-mechanical calculations of positron-impact ionization. Another form of Thomson's scaling law is presented in Figs. 13 and 14 by multiplying the reduced total cross section by u_i^2, where the universal curve becomes almost a straight line except near threshold. We emphasize that the apparent deviations of the H I and He II curves from the universal curve, which are better seen in Fig. 12, are due to the screening effect and the apparent deviations of the Fe XXVI and Ag XLVII curves from the universal curve, which are better seen in Fig. 13, are due to the relativistic effect.

Starting from a relativistic formulation, we arrive at an exact expression for the transition matrix element of positron-impact ionization. This transition matrix element is then reduced in the two-potential formalism. Finally, the distorted-wave approximation is made for the final-state wave function. Two models are used for the distorting potentials for the scattered positron and ejected electron. Although the screening effect between the scattered positron and ejected electron is only treated approximately by using distorted waves for the final-state wave function, the contribution arising from the screening effect may be estimated by the difference between models TPDW01 and TPDW11. The relativistic effect is also studied by comparison with cross sections in the nonrelativistic limit. We conclude that the screening effect is more significant for ions with low nuclear charge, and the relativistic effect is more significant for ions with high nuclear charge. The polarization of the electron density induced by the positron has a small effect on the total cross sections for H I and can be neglected for higher-Z ions. Results presented in this paper provide a systematic exposition of positron-impact ionization of hydrogen and ions in the hydrogen isoelectronic sequence and reveal some of the interesting features in the positron-impact ionization.

ACKNOWLEDGMENTS

This work was supported in part by the Atomic Energy Council and the National Science Council of the Republic of China under Grant No. NSC81-0208-M001-10.

*Present address: Division of General Education, National Taiwan Ocean University, Keelung, Taiwan 202, R.O.C.

[1] P. G. Burke and A. Taylor, Proc. R. Soc. London Ser. A **287**, 105 (1965).

[2] A. S. Ghosh, P. S. Mazumdar, and M. Basu, Can. J. Phys. **63**, 621 (1985).

[3] K. K. Mukherjee, N. R. Singh, and P. S. Mazumdar, J. Phys. B **22**, 99 (1989).

[4] K. K. Mukherjee, K. B. Choudhury, N. R. Singh, P. S. Mazumdar and S. Brajamani, Can. J. Phys. **68**, 249 (1990).
[5] A. Ohsaki, T. Watanabe, K. Nakanishi, and K. Iguchi, Phys. Rev. A **32**, 2640 (1985).
[6] A. E. Wetmore and R. E. Olson, Phys. Rev. A **34**, 2822 (1986).
[7] H. Klar, J. Phys. B **14**, 4165 (1981).
[8] R. I. Campeanu, D. Fromme, G. Kruse, R. P. McEachran, L. A. Parcell, W. Raith, G. Sinapius, and A. D. Stauffer, J. Phys. B **20**, 3557 (1987).
[9] G. Spicher, B. Olsson, W. Raith, G. Sinapius, and W. Sperber, Phys. Rev. Lett. **64**, 1019 (1990).
[10] R. I. Campeanu, R. P. McEachran, and A. D. Stauffer, J. Phys. B **20**, 1635 (1987).
[11] M. Charlton, Phys. Scripta **42**, 164 (1990).
[12] S.-W. Hsu, T.-Y. Kuo, C.-M. J. Chen, and K.-N. Huang, Phys. Lett. A **167**, 277 (1992).
[13] K.-N. Huang, Phys. Rev. A **28**, 1869 (1983); K.-N. Huang, Chin. J. Phys. **25**, 156 (1987).
[14] M. L. Goldberger and K. M. Watson, *Collision Theory* (Wiley, New York, 1965), Chap. 5.
[15] K.-N. Huang, Nucl. Instrum. Methods A **262**, 156 (1987); H.-C. Kao, T.-Y. Kuo, H.-P, Yen, C.-M. Wei, and K.-N. Huang, Phys. Rev. A **45**, 4646 (1992).
[16] A. Temkin and J. C. Lamkin, Phys. Rev. **121**, 788 (1961).
[17] J. J. Thomson, Philos. Mag. **23**, 449 (1912).